Cellulose Acetate/Carbon Nanotube Composites by Melt Mixing

A. Delgado-Lima, M. C. Paiva* and A. V. Machado

Institute of Polymers and Composites/I3N, University of Minho, Azurém, 4800-0581 Guimarães, Portugal

Received October 15, 2016; Accepted January 14, 2017

ABSTRACT: Cellulose acetate (CA) is produced from a natural polymer and presents excellent properties, finding applications in a variety of areas. Unlike cellulose, CA is melt processable and may be molded into parts and formed into fibers or films. In this context, the production of conductive CA composites that may be processable and integrated into parts to provide specific functionalities is an area of increasing interest. The present work aims to prepare electrically conductive composites based on CA and carbon nanotubes (CNTs) by melt mixing. The nanocomposites were produced with pure and pyrrolidine-functionalized nanotubes, using a batch mixer and a twin-screw extruder. The morphology of carbon nanotube dispersion, the rheological behavior and the electrical conductivity of the final composites were evaluated. Rheological percolation was achieved for the composites with 0.5 wt% of CNT—both pure and functionalized—produced by extrusion; while electrical percolation was observed only for the composites with pure CNT.

KEYWORDS: Cellulose acetate, carbon nanotubes, rheology, morphology, dispersion, electrical conductivity

1 INTRODUCTION

Over the years, the extensive production of conventional/non-biodegradable polymers has brought along with it environmental issues related to plastic waste management, which could be potentially solved by its replacement with biodegradable polymers [1–3]. Due to the increasing demand for environmentally friendly materials, biodegradable polymers and green processing techniques have attracted attention and their applications have opened up a wider range of sectors besides medical, tissue engineering, agriculture and biotechnology, including electronics, automobile and construction [2, 4, 5]. Cellulose is a biodegradable polymer with a highly crystalline structure that is very difficult to melt process and is frequently substituted by derivatives such as cellulose acetate (CA) [6, 7]. One of the attractive aspects of CA is that it is a melt processable polymer with excellent mechanical properties that may be processed by current industrial polymer melt processing techniques [8, 9]. Although CA biodegradability is a controversial subject among some authors, it is currently recognized as a biodegradable polymer within the scientific community [10–12]. Like the other polymers, it may reach tailored properties through composite preparation, using specific reinforcements to convey the target properties [13, 14]. Carbon nanotubes (CNTs) are a class of carbon-based nanoparticles with high electrical conductivity and excellent mechanical properties, frequently used to prepare electrically conductive polymer nanocomposites [14–16].

The achievement of electrical conductivity on polymer/CNT nanocomposites at low incorporation ratios requires the establishment of a conductive pathway throughout the matrix forming a percolating network, which depends on the CNT dispersion state [17, 18]. The main objective is to achieve good dispersion of the CNT in the polymer matrix during nanocomposite preparation and to establish strong interfacial bonding, simultaneously developing a percolating network and enhancing the composite mechanical properties [14, 19, 20]. However, when incorporated into a polymer matrix the CNTs have a strong tendency to agglomerate due to their physical entanglement and to van der Waals interactions among them, hindering their efficient wetting with the melted polymer and decreasing the effective stress transfer from the polymer to the CNTs, thus limiting the improvement in composite properties [21]. Enhancement of the polymer/CNT interactions has been achieved through CNT surface modification using a range of chemical and physical

*Corresponding author: mcpaiva@dep.uminho.pt

DOI: 10.7569/JRM.2017.634104

approaches, frequently based on treatment with strong oxidizing acids, causing CNT breakage and reducing their aspect ratio, consequently leading to a loss of CNT and composite properties [20].

Several polymers have been used to prepare CNT nanocomposites, but there are few examples in the literature concerning cellulose acetate, particularly through melt compounding. Li *et al.* [22] prepared CA/CNT nanocomposites by melt compounding with as-received CNT and with CNT functionalized with carboxylic groups (COOH). They demonstrated the establishment of a specific interaction between the acid group and the CA ester groups, that leads to improved interfacial adhesion, as well to a higher thermal stability and dynamic mechanical properties, when compared to the nanocomposites prepared with as-received CNT [22]. Despite the enhancement of the thermal and mechanical properties, the CNT acid functionalization showed a negative effect on the electrical properties of the nanocomposite. The electrical volume resistivity of the functionalized CNTs was higher and could be attributed to the deterioration of the graphene structure during the aggressive functionalization [22]. Despite this example, most of the literature on CA/CNT nanocomposites concerns solvent-based composite preparation techniques, which are usually less environmentally friendly. Gang Ke [23, 24] covalently modified CNT with CA using 2,4,6-trichloro-1,3,5-triazine as an intermediate to prepare a potential material to be used in applications that need specific sorption and insulation, such as cigarette filters. Luo *et al.* [25], Ahmad *et al.* [26] and Badawi *et al.* [27] have also incorporated CNT into cellulose acetate in the form of membranes. The first combined electrospinning and layer-by-layer techniques to achieve a material for tissue engineering applications, while Ahmad *et al.* [26] and Badawi *et al.* [27] prepared membranes for CO_2/N_2 gas separation and water filtration, respectively, by phase inversion with functionalized CNT.

Therefore, the main goal of the present study is to investigate the effect of incorporating as-received CNT and pyrrolidine-functionalized CNT (CNTNH) in the preparation of cellulose acetate nanocomposites, as well as the effect caused by the preparation of the nanocomposites using different melt processing techniques—a batch process (Haake intensive mixer) and a continuous process (twin-screw extrusion).

2 EXPERIMENTAL

2.1 Materials

Multiwall carbon nanotubes (NC 7000) were obtained from Nanocyl SA, Belgium. According to the supplier, these CNTs were produced via catalytic carbon vapor deposition (CCVD), achieving typical average diameters and lengths of 9.5 nm and 1.5 µm respectively. Cellulose acetate with an acetylation degree of 39.8 wt% (Mn ≈ 50 000 g/mol) was employed as polymeric matrix and supplied by Sigma-Aldrich.

2.2 Sample Preparation

2.2.1 Nanocomposites

The CNTs were covalently functionalized with pyrrolidine groups under mild reaction conditions as described elsewhere [28]. The reaction conditions used for the functionalization were 250 °C for 3 hours. This procedure was used to test the effect of functionalization on the dispersion and compatibilization of the CNT in the CA matrix.

The nanocomposites were prepared by melt compounding using two approaches: i) an intensive batch mixer Haake Rheomix 600 OS, v = 60 cm^3 (HK) and ii) a MicroLab co-rotating twin-screw extruder Rondol C3045 (ME) with L/D = 20/1, nominal screw diameter = 10 mm, die = 2 mm, and feeding rate of 1.37 g/min. The screw profile is composed of two main zones, the drag, which also compromises the feed zone with conveying elements, and the mixing zone with kneading elements staggered at 60° and 90° (Figure 1). The conveying elements are known to control the speed of transport and distributive mixing, while the kneading elements induce chaotic mixing from different hydrodynamic stress levels, promoting variable scales

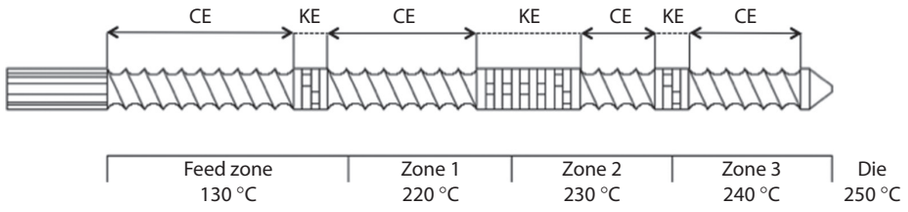

Figure 1 Screw configuration and temperature profile; CE – conveying elements; KE – kneading elements.

of distributive/dispersive mixing [29]. Cellulose-based nanocomposites with 0.1 and 0.5 wt% of as-received and functionalized CNTs were prepared in both equipment. For the batch process a temperature of 230 °C and 100 rpm was applied for 8 minutes. Similar samples were produced in the mini-extruder at a screw speed of 100 rpm and using the temperature profile presented in Figure 1. In both cases, CA and CNT were previously dried in an oven, weighted and mixed in powder form before processing.

2.2.2 *Preparation of Samples by Compression Molding*

The characterization of the electrical and rheological properties of the composites prepared by both techniques was performed on compression-molded plates and disks, produced on a Moore hydraulic heated press. For the rheological measurements, the composites prepared in both equipment were molded into disks with 25 mm diameter and 1 mm thickness. For the electrical measurements, rectangular plates with 85 × 75 × 1 (length × width × thickness, mm^3) were prepared for the batch mixer composites. The electrical resistivity of the composites prepared on the mini-extruder was measured directly on the extruded filaments. The compression molding of plates and disks was performed at 250 °C applying a maximum pressure of 25 bar and cooling under pressure until the press temperature dropped to 60 °C.

2.3 Characterization

The dispersion of the CNT agglomerates formed during processing was analyzed by optical microscopy using a BH2 Olympus transmission microscope. The analysis procedure was described elsewhere [30]. Thin sections of 3-μm thickness were cut from the extruded filaments perpendicularly to the filament axis direction using an ultramicrotome Leica EM UC6 equipped with a glass knife with an angle of 45°. Samples were also cut along the filament axis direction and the analysis results showed a comparable agglomerate morphology to the perpendicular direction, indicating that no considerable orientation effects were induced during extrusion. The microscope images were collected with a Leica DFC280 camera coupled to the microscope, using a 20x objective and 3.3x eyepiece. The quantitative particle analysis was performed using Leica Application Suite 4.4 digital image processing software, and a minimum area of 8.80×10^4 μm^2 from at least 4 different cut sections was analyzed for each sample and composition. The data collected from the image processing were used to plot the statistical distribution of CNT agglomerates, provided by the representation of the cumulative agglomerate area ratio distribution, F, against the agglomerate area, A_i. F is calculated as the variation of the agglomerate area ratio, obtained by ranking the areas of the n agglomerates measured in increasing order of magnitude, and calculating each area ratio, F_j, from the smaller to the larger agglomerate, as described in Equation 1 [30, 31]. The numerator $\sum_{i=1}^{j} A_i$ represents the sum of the agglomerate areas from the smaller to the j^{th} agglomerate, and the denominator is the total agglomerate area, $= \sum_{i=1}^{n} A_i$, where n represents the total number of agglomerates.

$$F_j = \frac{\sum_{i=1}^{j} A_i}{A} \times 100 \quad (1)$$

Cryofractured nanocomposites sputtered with a gold/platinum mixture were observed by scanning electron microscopy (SEM) on a FEI Nova NanoSEM 200, at an acceleration voltage of 5.00 kV in secondary electron image mode. The rheological measurements were performed using a rotational rheometer (AR-G2, TA Instruments), with 25 mm diameter parallel plates with a gap of 1 mm, in a frequency range from 1×10^{-2} to 1×10^2 Hz, at 240 °C. A constant strain of 5% was used after determination of the linear viscoelastic region by an amplitude sweep. The disks were dried for at least 4 h at 80 °C before each measurement. The nanocomposites volume resistivity was measured using a two-probe method by applying a voltage between −10 and 10 mV on opposite sides of the sample and measuring the resultant current through it using a Keithley 6487 picoammeter/voltage source at room temperature. Previous to the assays, the ends of the filaments from the ME processing (area approximately 0.02 cm^2 and lengths between 1.2–1.7 cm) were coated with a silver conductive lacquer, where the probes contacted the sample. The electrical contacts on the sample plates prepared in the batch mixer were obtained through gold coating by thermal evaporation. The resistivity was calculated based on Ohm's law and taking into account the geometrical factors. The electrical resistivity of the filaments was calculated using the equation:

$$R = \frac{\rho . L}{s} \quad (2)$$

where R is the filament resistance that can be calculated from the I-V curve slope, ρ the resistivity of the material, L the length of the filament and s the cross-section area.

The electrical resistivity of the plates was also calculated from Equation 2, where s is the electrode area

(constant = 5 mm), and *L* corresponds to the average thickness of the sample.

3 RESULTS AND DISCUSSION

Figure 2 shows representative optical microscopy images of the samples with 0.5 wt% of as-received and functionalized CNT, both prepared in the batch mixer and in the mini-extruder. The analysis of the optical microscopy images allowed the quantification of the non-dispersed CNT fraction, which is relevant as it correlates with the dispersion level achieved [29]. The most striking difference is observed between the as-received and functionalized CNT, rather than between the samples processed with different techniques. All the composites prepared with as-received CNT showed a smaller number of agglomerates compared to the composites with CNTNH.

The statistical analysis of the CNT agglomerate areas confirms that a much larger number of agglomerates is found in the composites with CNTNH, possibly due to higher agglomerate cohesion in spite of the stronger CNTNH/polymer interactions that may form [21]. The number of agglomerates is almost double that of the composites prepared in the HK, relative to those prepared in the ME (Table 1). The agglomerate area ratio, A_R, defined as the sum of all the agglomerate areas measured divided by the total composite area analyzed, provides a good indicator of the overall dispersion achieved. Smaller A_R values indicate that less CNT agglomerates remain in the composite, and thus a higher fraction of CNT was effectively dispersed. The A_R results presented in Table 1 show that the CNT dispersion in CA was 3–4 times more efficient compared to the dispersion of CNTNH. The processing in the ME was more effective for CNT dispersion compared to the processing in the HK. Figure 3 presents *F*, the cumulative agglomerate area ratio distribution as a function of the agglomerate area, for all the nanocomposites.

Keeping in mind that the as-received CNTs were more effectively dispersed than the CNTNH by both processing methods, but attending to their agglomerates size distribution, Figure 3 shows that the nanocomposites processed in the ME and the CNTNH composite processed on the HK have a larger population of small agglomerates, with 70% of the total population presenting agglomerate areas smaller than 28 μm^2. It is observed that processing with the HK always leaves a considerable fraction of remaining large agglomerates for pure and functionalized CNT composites. Thus, the shear rate applied to the polymer melt along the ME screw length, combined with the intensive mixing in the kneading blocks, results in a more efficient rupture of the large CNT agglomerates into smaller ones.

While optical microscopy provides images of the nanocomposites CNT agglomerate phase, SEM images

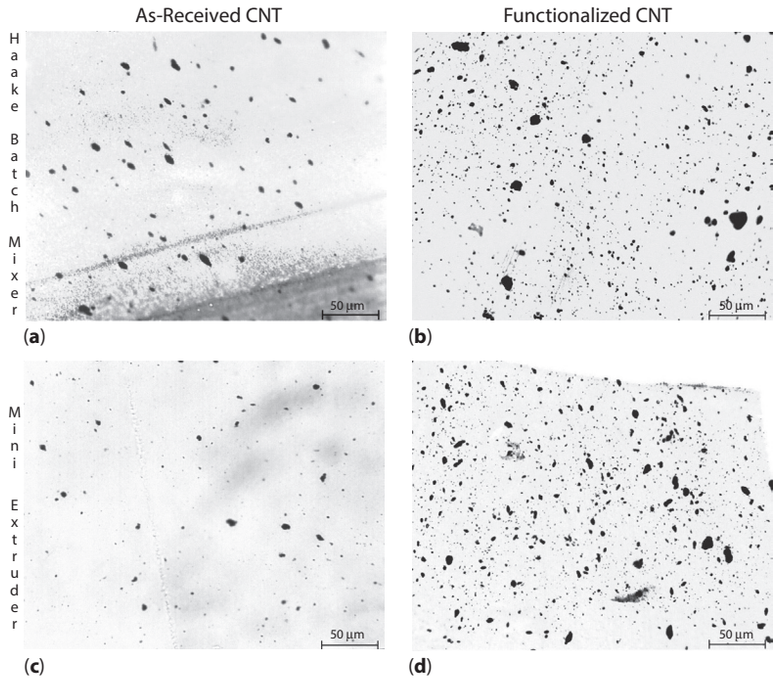

Figure 2 Optical microscopy images of the samples prepared in the batch mixer (**a**) 0.5CNT(HK), (**b**) 0.5CNTNH(HK); and in the mini-extruder (**c**) 0.5CNT(ME), (**d**) 0.5CNTNH(ME).

Table 1 Optical microscopy analysis.

Samples	Agglomerate area ratio, A_R (%)	Number of agglomerates/per unit area (mm^{-2})	Maximum agglomerate area (μm^2)	$A\chi 70\%$ (μm^2) [a)]
0.5CNT(ME)	1.38	931	90.7	28.2
0.5CNTNH(ME)	4449	260.3	27.6	6.73
0.5CNT(HK)	2.08	1741	386.0	69.5
0.5CNTNH(HK)	6.01	8792	775.2	26.9

[a)]Maximum area of the agglomerates contained in 70% of the total agglomerate area.

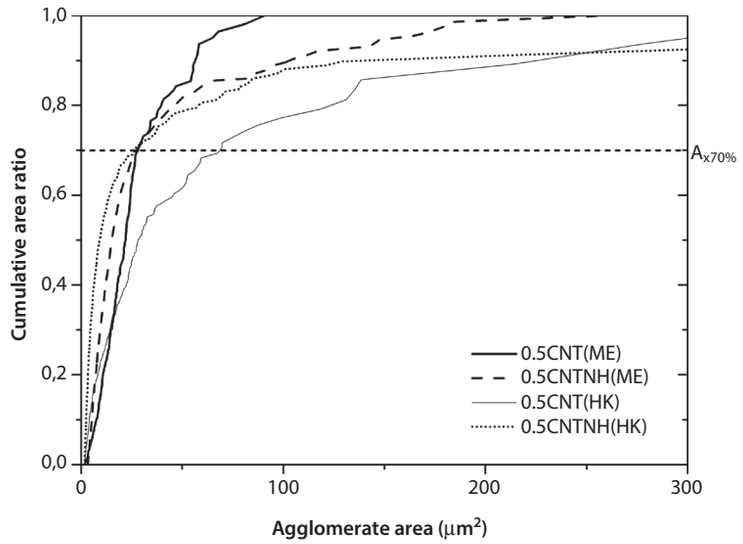

Figure 3 Cumulative agglomerate area ratio distribution.

of their cryofractured surfaces show the dispersed CNT, i.e., the CNT fraction that is individually dispersed across the CA matrix. Figure 4 depicts typical SEM micrographs showing the presence of individually dispersed CNT across the composites. The micrographs evidence a higher concentration of dispersed CNT, either as-received or functionalized, on the composites processed by ME, compared to HK.

The pyrrolidine groups on the CNTNH surface are expected to have good affinity to the CA matrix through hydrogen bonding, as represented in Figure 5. These enhanced interactions are expected to result in a stronger CA/CNTNH interface, thus improving the composite mechanical properties. However, the CNTNH surface functionalization does not necessarily facilitate the nanotube dispersion in the polymer melt. In fact, the agglomerates of functionalized CNTNH may be more stable and difficult to break into smaller agglomerates compared to those of pristine CNT. If this is the case, higher stress levels will be required to break the stable agglomerates into consecutively smaller ones, otherwise a lower overall dispersion will be observed, as well as the survival of large agglomerates. However, the higher affinity between CNTNH and the CA matrix may enhance the CNT dispersion through erosion from the agglomerates surface into the bulk polymer melt, thus leading to a considerable individual CNTNH dispersion into the CA matrix.

As shown by optical and electron microscopies, the processing method and CNT treatment has a strong influence on the CNT dispersion in CA. It is well known that the nanoparticle dispersion state will affect the rheological behavior of the nanocomposites [21, 32]. In the present work, the CA and nanocomposites dynamic rheological properties were assessed by measuring the complex viscosity (η^*), the storage (G′) and loss (G″) modulus as a function of frequency (ω), and calculating tan (δ), the ratio G″/G′, as represented in Figure 6.

It is well documented that for polymer nanocomposites the values of G′ and G″ increase with CNT concentration, evidencing the contribution of CNT/polymer interactions to the melt elastic

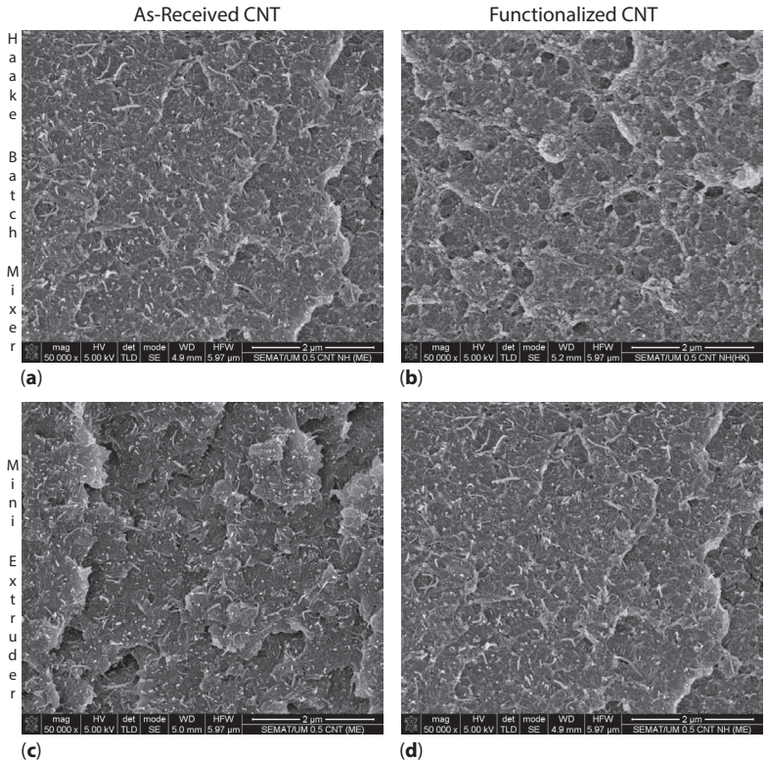

Figure 4 Representative SEM micrographs of the nanocomposites processed in the batch mixer (**a**) 0.5CNT(HK), (**b**) 0.5CNTNH(HK); and in the mini-extruder (**c**) 0.5CNT(ME), (**d**) 0.5CNTNH(ME).

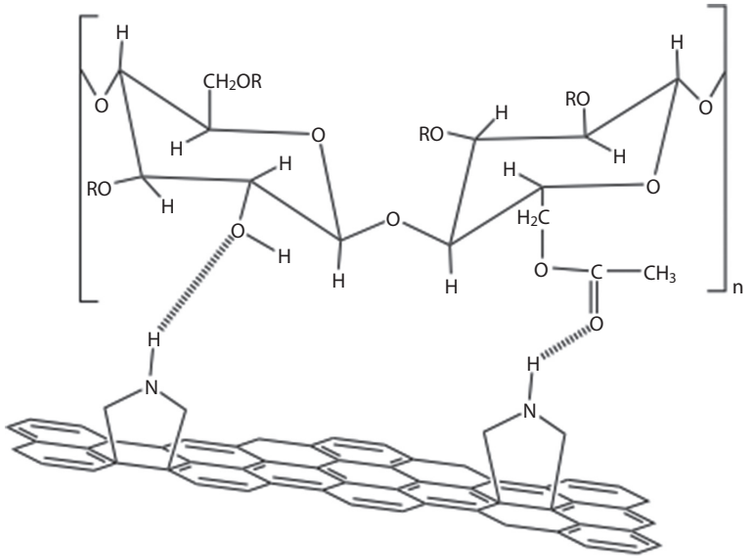

Figure 5 CA/CNTNH interaction through hydrogen bonding (R = $COCH_3$ or R = H).

behavior [32, 33]. The η^* of the CNT composites is higher than that of the polymer, the latter presenting a Newtonian plateau at low frequencies. This plateau disappears for composites containing a well-dispersed CNT network capable of imposing the elastic behavior across the frequency range. In the present work, the deviation from the Newtonian plateau behavior was observed for the composites with 0.5 wt% of CNT and CNTNH prepared by ME (Figure 6a,b). A clear decrease in the slope

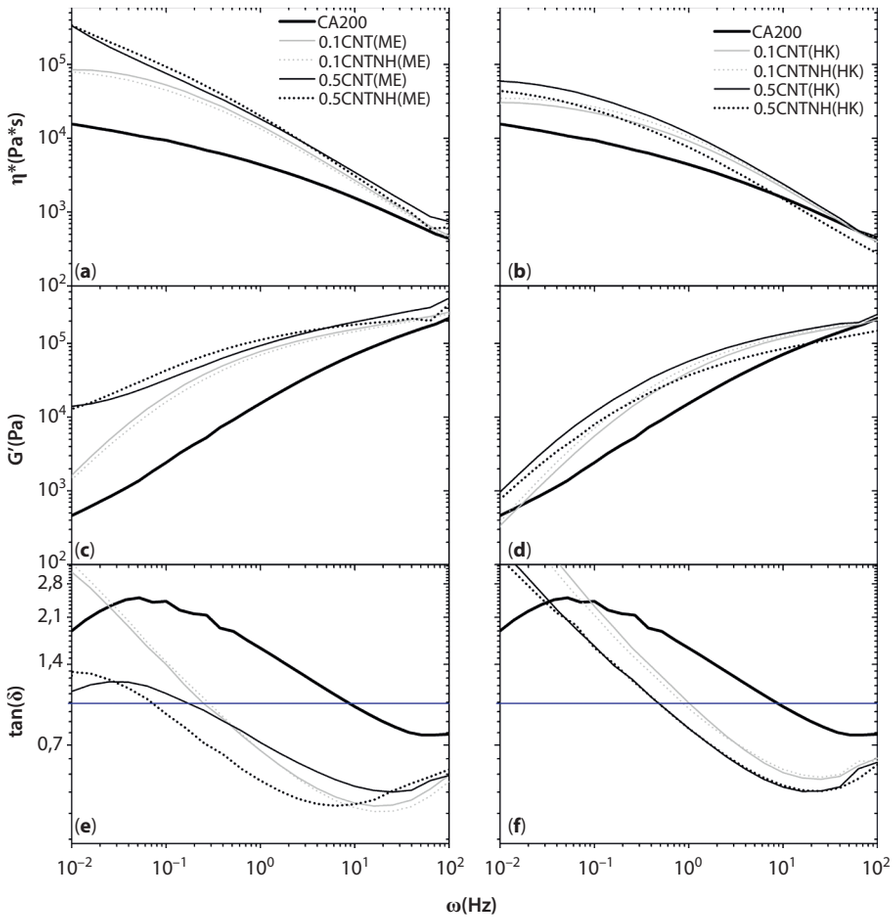

Figure 6 Complex viscosity (**a** and **b**), Storage modulus (**c** and **d**) and tan(δ) (**e** and **f**) of CA and nanocomposites prepared by melt mixing (left) and in the Haake mixer (right).

of G′ vs. ω was observed only for these composites (Figure 6c,d). This effect was reported by Du *et al*. [34], concluding that good CNT dispersion and long polymer chains induce higher restraints to the polymer mobility leading to a lower slope of G′ vs. ω in the low frequency range, and higher G′ values at low frequencies. This also indicates a better load transfer between the nanotube network and the polymer [35].

The variation of tan (δ) with frequency provides relevant information about the damping characteristics of the composites relative to the pure polymer. The lower values of tan (δ) measured for the nanocomposites indicate higher elastic behavior of the polymer melt (higher G′), interpreted as hindrance of polymer relaxation in the presence of the CNT network [32]. Figure 6e and 6f show that CA undergoes a transition from elastic to viscous behavior at a frequency near 10 Hz, at which tan (δ) = 1, and thus G″ > G′ for higher frequencies. A shift of this transition to lower frequencies was observed for all composites. Those prepared in the HK shifting in ω by one order of magnitude, while those prepared in the ME shifting by nearly two orders of magnitude. Below this frequency value (at tan (δ) = 1) the dissipative behavior of the melt increases with decreasing ω for CA and composites, except for the 0.5 wt% CNT and CNTNH prepared by ME, that nearly stabilizes around a tan (δ) ≈ 1 (Figure 6e,f).

In conclusion, the rheological data indicate a clear influence of the CNT presence in the CA melt behavior. However, only the ME composites with 0.5 wt% CNT and CNTNH presented the rheological response characteristic of the establishment of a CA/CNT percolated network.

The electrical resistivity of the nanocomposites was measured to evaluate if the electrical percolation was reached. The rheological and electrical percolation are closely related, although the rheological percolation is reported to be attained at lower CNT content [34, 35]. The electrical resistivity results obtained for CA and its composites are presented in Figure 7.

Higher electrical resistivity was obtained for composites with similar CNT content produced in HK

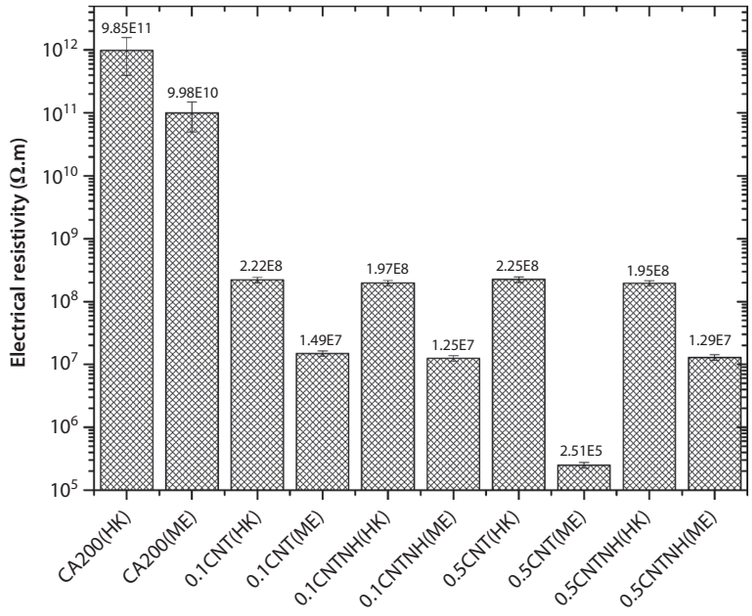

Figure 7 Electrical resistivity results.

relative to ME. This result correlates with the poorer CNT dispersion observed for HK composites by optical microscopy. The insulating character of the CA polymer matrix was confirmed by the high resistivity obtained, near the limit of the measuring equipment.

The composites prepared with 0.1 wt% CNT show a significant reduction of electrical resistivity by three orders of magnitude relative to the polymer. The composite prepared in the ME containing 0.5 wt% of as-received CNT presented the lower resistivity, already in the semiconducting range, thus reaching both rheological and electrical percolation thresholds. These results are in line with the efficient CNT dispersion observed by optical and electron microscopies. However, the composite with 0.5 wt% CNTNH (ME) did not reach the electrical percolation threshold, probably due to the poorer CNT dispersion observed by optical microscopy.

4 CONCLUSION

The present study demonstrated the relevance of the processing method and chemical functionalization with pyrrolidine on the dispersion of the MWCNT in the CA, and consequently on the melt and solid-state properties.

The morphological analysis showed that smaller CNT agglomerates were formed and better dispersion was achieved when the melt mixing was performed by twin-screw extrusion. The functionalization of the CNT did not facilitate the dispersion of their agglomerates in the polymer. However, rheological percolation was observed for the composites with 0.5 wt% CNT, either pure or functionalized, prepared by extrusion. The poorer dispersion of the functionalized CNT limited the composite electrical conductivity. However, a large reduction of the electrical resistivity was found at a low CNT concentration, 0.5 wt% CNT, presenting an electrical conductivity of 2.5×10^5 S/m.

ACKNOWLEDGMENTS

The authors acknowledge the Portuguese Foundation of Science and Technology (SFRH/BD/81711/2011 and PEst-C/CTM/LA0025/2011) and n-SteP – Nanostructured Systems for Tailored Properties, with reference NORTE-07-0124-FEDER-000039, supported by the Programa Operacional Regional do Norte (ON.2).

REFERENCES

1. R.-J. Müller, *Biodegradability of Polymers: Regulations and Methods for Testing*, John Wiley and Sons, Inc, New Jersey, Published online (2005).
2. W. Amass, A. Amass, and B. Tighe, A review of biodegradable polymers: Uses, current developments in the synthesis and characterization of biodegradable polyesters, blends of biodegradable polymers and recent advances in biodegradation studies. *Polym. Int.* **47**, 89–144 (1998).
3. J.W. Rhim and P.K. Ng, Natural biopolymer-based nanocomposite films for packaging applications. *Crit. Rev. Food Sci. Nutr.* **47**, 411–433 (2007).

4. I. Vroman and L. Tighzert, Biodegradable polymers. *Materials* **2**, 307–344 (2009).
5. Y. Ikada and H. Tsuji, Biodegradable polyesters for medical and ecological applications. *Macromol. Rapid Commun.* **21**, 117–132 (2000).
6. Y. Li, M. Wu, R. Liu, and Y.M. Huang, Cellulose-based solid–solid phase change materials synthesized in ionic liquid. *Sol. Energ. Mat. Sol. Cells* 93, 1321–1328 (2009).
7. G.W. Jeon, J.-E. An, and Y.G. Jeong, High performance cellulose acetate propionate composites reinforced with exfoliated graphene. *Compos. Part B: Eng.* 43, 3412–3418 (2012).
8. G. Számel, A. Domján, S. Klébert, and B. Pukánszky. Molecular structure and properties of cellulose acetate chemically modified with caprolactone. *Eur. Polym. J.* **44**, 357–365 (2008).
9. H.O. Ghareeb, F. Malz, P. Kilz, and W. Radke, Molar mass characterization of cellulose acetates over a wide range of high DS by size exclusion chromatography with multi-angle laser light scattering detection. *Carbohydr. Polym.* **88**, 96–102 (2012).
10. R.K.D.E. Samios and J.V. Dawkins, Preparation, characterization and biodegradation studie on cellulose acetates with varying degrees of substitution. *Polymer* **38**, 3045–3054 (1997).
11. J. Puls, S.A. Wilson, and D. Hölter, Degradation of Cellulose acetate-based materials: A review. *J. Polym. Environ.* **19**, 152–165 (2010).
12. C.M. Buchanan, R.M. Gardner, and R.J. Komarek, Aerobic biodegradation of cellulose acetate. *J. Appl. Polym. Sci.* **47**, 1709–1719 (1993).
13. N.G. Sahoo, S. Rana, J.W. Cho, L. Li, andS.H. Chan, Polymer nanocomposites based on functionalized carbon nanotubes. *Prog. Polym. Sci.* **35**, 837–867 (2010).
14. Z. Spitalsky, D. Tasis, K. Papagelis, and C. Galiotis, Carbon nanotube–polymer composites: Chemistry, processing, mechanical and electrical properties. *Prog. Polym. Sci.* **35**, 357–401 (2010).
15. F.-L. Jin and S.-J. Park, A review of the preparation and properties of carbon nanotubes-reinforced polymer compositess. *Carbon Lett.* **12**, 57–69 (2011).
16. W. Bauhofer and J.Z. Kovacs, A review and analysis of electrical percolation in carbon nanotube polymer composites. *Compos. Sci. Technol.* **69**, 1486–1498 (2009).
17. L. Valentini, D. Puglia, and J.M. Kenny, Methods for improving the integration of functionalized carbon nanotubes in polymers, in *Carbon Nanotube-Polymer Composites*, D. Tasis (Ed.), chap. 8, pp. 234–252. Royal Society of Chemistry, London, UK (2013).
18. G. Kasaliwal, T. Villmow, S. Pegel, and P. Pötschke, Influence of material and processing parameters on carbon nanotube dispersion in polymer melts, in *Polymer Carbon Nanotube Composites: Preparation, Properties and Applications*, T. McNally, P. Pötschke (Eds.), part 1, chap. 4, Woodhead Publishing Limited, Cambridge, UK (2011).
19. P. Liu, Modifications of carbon nanotubes with polymers. *Eur. Polym. J.* **41**, 2693–2703 (2005).
20. R. Araújo, M.C. Paiva, M.F. Proença, and C.J.R. Silva, Functionalization of carbon nanofibres by 1,3-dipolar cycloaddition reactions and its effect on composite properties. *Compos. Sci. Technol.* **67**, 806–810 (2007).
21. I. Alig, P. Pötschke, D. Lellinger, T. Skipa, S. Pegel, G.R. Kasaliwal, and T. Villmow, Establishment, morphology and properties of carbon nanotube networks in polymer melts. *Polymer* **53**, 4–28 (2012).
22. M. Li, I.-H. Kim, and Y.G. Jeong, Cellulose acetate/multiwalled carbon nanotube nanocomposites with improved mechanical, thermal, and electrical properties. *J. Appl. Polym. Sci.* **118**, 2475–2481 (2010).
23. G. Ke, Homogeneous modification of carbon nanotubes with cellulose acetate. *Chin. Chem. Lett.* **20**, 1376–1380 (2009).
24. G. Ke, A novel strategy to functionalize carbon nanotubes with cellulose acetate using triazines as intermediated functional groups. *Carbohydr. Polym.* **79**, 775–782 (2010).
25. Y. Luo, S. Wang, M. Shen, R. Qi, Y. Fang, R. Guo, H. Cai, X. Cao, H. Tomas, M. Zhu, and X. Shi, Carbon nanotube-incorporated multilayered cellulose acetate nanofibers for tissue engineering applications. *Carbohydr. Polym.* **91**, 419–427 (2013).
26. A.L. Ahmad, Z.A. Jawad, S.C. Low, and S.H.S. Zein, A cellulose acetate/multi-walled carbon nanotube mixed matrix membrane for CO_2/N_2 separation. *J. Membr. Sci.* **451**, 55–66 (2014).
27. N. El Badawi, A.R. Ramadan, A.M.K. Esawi, and M. El-Morsi, Novel carbon nanotube–cellulose acetate nanocomposite membranes for water filtration applications. *Desalination* **344**, 79–85 (2014).
28. M.C. Paiva, F. Simon, R. Novais, T. Ferreira, M. Proença, W. Xu, and F. Besenbacher, Controlled functionalization of carbon nanotubes by a solvent-free multicomponent approach. *ACS Nano* **4**, 7379–7386 (2010).
29. R.M. Novais, F. Simon, P. Pötschke, T. Villmow, J.A. Covas, and M.C. Paiva, Poly(lactic acid) composites with poly(lactic acid)-modified carbon nanotubes. *J. Polym. Sci. A: Polym. Chem.* **51**, 3740–3750 (2013).
30. R.M. Novais, J.A. Covas, and M.C. Paiva, The effect of flow type and chemical functionalization on the dispersion of carbon nanofiber agglomerates in polypropylene. *Compos. Part A: Appl. Sci. Manuf.* **43**, 833–841 (2012).
31. C. Vilaverde, R.M. Santos, M.C. Paiva, and J.A. Covas, Dispersion and re-agglomeration of graphite nanoplates in polypropylene melts under controlled flow conditions. *Compos. Part A: Appl. Sci. Manuf.* **78**, 143–151 (2015).
32. A.K. Kota, B.H. Cipriano, M.K. Duesterberg, A.L. Gershon, D. Powell, S.R. Raghavan, and H.A. Bruck, Electrical and rheological percolation in polystyrene/MWCNT nanocomposites. *Macromolecules* **40**, 7400–7406 (2007).
33. P. Pötschke, T.D. Fornes, and D.R. Paul, Rheological behavior of multiwalled carbon nanotube/polycarbonate composites. *Polymer* **43**, 3247–3255 (2002).
34. F. Du, R.C. Scogna, W. Zhou, S. Brand, J.E. Fischer, and K.I. Winey, Nanotube networks in polymer nanocomposites: Rheology and electrical conductivity. *Macromolecules* **37**, 9048–9055 (2004).
35. M. Moniruzzaman and K.I. Winey, Polymer nanocomposites containing carbon nanotubes. *Macromolecules* **39**, 5194–5205 (2006).

